

Gradient Starvation: A Learning Proclivity in Neural Networks

Mohammad Pezeshki^{1,2}, Sékou-Oumar Kaba^{1,3}, Yoshua Bengio^{1,2},
 Aaron Courville^{1,2}, Doina Precup^{1,3,4}, and Guillaume Lajoie^{1,2}

¹ Mila, ² Université de Montréal, ³ McGill University, ⁴ Google DeepMind

Abstract. We identify and formalize a fundamental gradient descent phenomenon resulting in a learning proclivity in over-parameterized neural networks. *Gradient Starvation* arises when cross-entropy loss is minimized by capturing only a subset of features relevant for the task, despite the presence of other predictive features that fail to be discovered. This work provides a theoretical explanation for the emergence of such feature imbalance in neural networks. Using tools from Dynamical Systems theory, we identify simple properties of learning dynamics during gradient descent that lead to this imbalance, and prove that such a situation can be expected given certain statistical structure in training data. Based on our proposed formalism, we develop guarantees for a novel regularization method aimed at decoupling feature learning dynamics, improving accuracy and robustness in cases hindered by gradient starvation. We illustrate our findings with simple and real-world out-of-distribution (OOD) generalization experiments.

1 Introduction

In 1904, a horse named *Hans* attracted worldwide attention due to the belief that it was capable of doing arithmetic calculations (Pfungst, 1911). Its trainer would ask Hans a question, and Hans would reply by tapping on the ground with its hoof. However, it was later revealed that the horse was only noticing subtle but distinctive signals in its trainer’s unconscious behavior, unbeknown to him, and not actually performing arithmetic.

An analogous phenomenon has been noticed when training neural networks (e.g. Ribeiro et al., 2016; Zhao et al., 2017; Jo and Bengio, 2017; Heinze-Deml and Meinshausen, 2017; Belinkov and Bisk, 2017; Baker et al., 2018; Gururangan et al., 2018; Jacobsen et al., 2018; Zech et al., 2018; Niven and Kao, 2019; Ilyas et al., 2019; Brendel and Bethge, 2019; Lapuschkin et al., 2019; Oakden-Rayner et al., 2020). State-of-the-art neural networks reportedly appear to focus on low-level **superficial correlations**, rather than more abstract and robustly informative features of interest (Beery et al., 2018; Rosenfeld et al., 2018; Hendrycks and Dietterich, 2019; McCoy et al., 2019; Geirhos et al., 2020). Neural networks learning to classify images only based on watermarks or latching on data compression artifacts are among the authors’ personal experiences.

The rationale behind this phenomenon is well known: Given strongly-correlated and fast-to-learn features in training data, gradient descent is biased towards learning them first. However, the precise conditions leading to such learning dynamics and how one might intervene to control this *feature imbalance* are not entirely understood. Recent work aims at identifying the reasons behind this phenomenon (Valle-Pérez et al., 2018; Nakkiran et al., 2019; Cao et al., 2019; Nar and Sastry, 2019; Jacobsen et al., 2018; Niven and Kao, 2019; Wang et al., 2019; Shah et al., 2020; Rahaman et al., 2019; Xu et al., 2019b; Hermann and Lampinen, 2020; Parascandolo et al., 2020; Ahuja et al., 2020b), while complementary work quantifies resulting shortcomings, including poor generalization to out-of-distribution (OOD) test data, reliance upon spurious correlations, and lack of robustness (Geirhos et al., 2020; McCoy et al., 2019; Oakden-Rayner et al., 2020; Hendrycks and Gimpel, 2016; Lee et al., 2018; Liang et al., 2017; Arjovsky et al., 2019).

In this paper, we argue that *Gradient Starvation*, first coined in Combes et al. (2018), is a leading cause for this *feature imbalance* in neural networks trained with cross-entropy.

Gradient Starvation refers to the phenomenon in which a neural network learns to capture statistically dominant features in the data while remaining invariant to the rest. Here, gradient decent updates the parameters, predominantly in directions that only capture these dominant features, thus “starving” the gradient from other potentially informative features.

Here we summarize our contributions:

- We provide a theoretical framework to study the learning dynamics of wide, over-parameterized neural networks trained with cross-entropy loss.
- Using the Legendre transformation of the loss (Eq. 12), we recast the learning dynamics to a dual space (Eq. 17).
- Using tools from dynamical systems theory, we study the coupled learning dynamics starting from exact solutions in uncoupled cases. With a perturbation analysis, we formalize “Gradient Starvation” (GS) in view of the coupling between the dynamics of orthogonal directions in the feature space (Thm. 2).
- We leverage our theoretical findings to introduce “Spectral Decoupling” (SD) (Eq. 25) and prove this simple regularizer helps to decouple learning dynamics (Eq. 27) and thus alleviates GS.
- Finally, we support our findings with encouraging empirical results on both simple and real-world examples. To ensure reproducibility, we provide a [Github repository](#) that contains the code to reproduce the results. Our findings are also summarized in a [blog post](#) that accompanies this paper.

2 Gradient Starvation: A simple demonstration

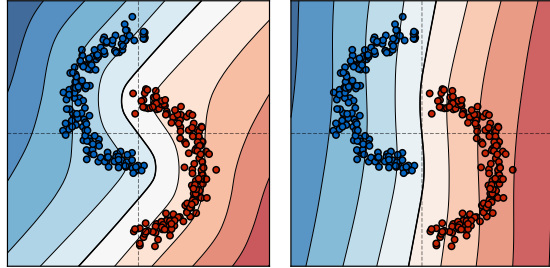


Fig. 1: Diagram illustrating the effect of gradient starvation in a simple 2-D classification task. Two different arrangements of the training data points, and the corresponding decision boundaries (black lines) are shown. Note that the only difference between the two arrangements is that in the one on the right, the two classes are linearly separable by a small margin. This small margin allows the network to discriminate confidently only along the horizontal axis and ignore the vertical axis.

We start with a simple illustration. Consider a 2-D classification task with a training set consisting of two classes, as shown in Figure 1. A two-layer ReLU network with 500 hidden units is trained with the cross-entropy loss for two different arrangements of the training points. The difference between the two arrangements is that the data is linearly separable with a small margin on the right plot. This small margin allows the network to achieve a negligible loss by only learning to discriminate along the horizontal axis, ignoring the other. We hypothesize that gradient starvation is responsible for the shape of the learned decision boundary on the right. Simply put, when one feature is learned faster than the others, the gradient contribution of examples containing that feature is diminished. This results in a lack of sufficient gradients as the training algorithm’s driving force and hence prevents any remaining features from learning.

We observe that training longer or using different regularizers, including weight decay (Krogh and Hertz, 1992), dropout (Srivastava et al., 2014), batch normalization (Ioffe and Szegedy, 2015), as well as changing the optimization algorithm to Adam (Kingma and Ba, 2014) or changing the network architecture or coordinate system, do not encourage the network to learn a curved decision boundary. (See Appendix A for more details.)

2.1 Consequences of Gradient Starvation

Lack of robustness. In the example above, even in the right plot, the training loss is nearly zero, and the network is very confident in its predictions. However, the decision boundary is located very close to the datapoints. This could lead to adversarial vulnerability as well as lack of robustness when generalizing to out-of-distribution data.

Excessive invariance. GS could also result in neural networks that are invariant to task-relevant changes in the input. In the example above, it is possible to obtain a data point with low probability under the data distribution, but that would still be classified with high confidence.

Implicit regularization. One might argue that according to Occam’s razor, a simpler decision boundary should generalize better. In fact, if both training and test sets share the same dominant feature (in this example, the feature along the horizontal axis), GS naturally prevents the learning of less dominant features that could otherwise result in overfitting. Therefore, depending on our assumptions on the training and test distributions, GS could also act as an implicit regularizer. We provide a discussion on the *implicit regularization* aspect of the GS in Section 5.

3 Theoretical Framework

3.1 Prelude

In this section, we study the learning dynamics of neural networks trained with cross-entropy loss. Particularly, we seek to decompose the learning dynamics along orthogonal directions in the feature space of neural networks.

Several works have introduced different decompositions of the learning process. Rahaman et al. (2019); Xu et al. (2019a); Ronen et al. (2019); Xu et al. (2019b) study the learning in the Fourier domain and show that low-frequency functions are learned earlier than high-frequency ones. Saxe et al. (2013); Advani et al. (2020); Gidel et al. (2019) provide closed-form equations for the dynamics of linear networks in terms of the principal components of the input covariance matrix. More recently, with the introduction of neural tangent kernel (NTK) (Jacot et al., 2018; Lee et al., 2019), a new line of research is to study the convergence properties of gradient descent for general neural networks (e.g. Allen-Zhu et al., 2019b; Mei and Montanari, 2019; Chizat and Bach, 2018; Du et al., 2018b; Allen-Zhu et al., 2019a; Huang and Yau, 2019; Goldt et al., 2019; Zou et al., 2020; Arora et al., 2019b; Vempala and Wilmes, 2019). Among them, Arora et al. (2019c); Yang and Salman (2019); Bietti and Mairal (2019) decompose the learning process along the principal components of the NTK and Cao et al. (2019) show that the corresponding eigenvalue determines the convergence rate along each component.

Most of the studies mentioned above focus on the particular squared-error loss. For a linearized network, the squared-error loss results in linear learning dynamics, which often admit an analytical solution. However, the de-facto loss function for many of the practical applications of neural networks is the cross-entropy. Using the cross-entropy as the loss function leads to significantly more complicated and non-linear dynamics, even for a linear neural network.

Here, we focus on studying the cross-entropy loss function in the linearized regime of NTK. Using a variational approximation of the loss and in the infinitesimal learning rate limit, we obtain a non-linear gradient flow system describing the learning process. We then decompose the learning in the basis of principal

components of the NTK and show that their dynamics are coupled in the general form. Using tools from perturbation theory, we identify properties of the system in specific cases, that we coin as the ‘‘Gradient Starvation’’: An increase in the dominancy (the corresponding singular value) of a leading feature (principal component of the NTK) reduces the learning of other features. Finally, we leverage our findings to introduce ‘‘Spectral Decoupling’’ and prove that this regularizer decouples the dynamics of each component.

See Appendix B for the missing details and the proofs.

3.2 Problem Setup

Let $\mathcal{D} = \{\mathbf{X}, \mathbf{y}\}$ denote a training set containing n datapoints $\mathbf{X} = [\mathbf{x}_1, \dots, \mathbf{x}_n] \in \mathbb{R}^{n \times d}$ and their corresponding class label $\mathbf{y} \in \{-1, +1\}^n$. Also let $\hat{\mathbf{y}}(\mathbf{X}) := f^{(L)}(\mathbf{X}) : \mathbb{R}^{n \times d} \rightarrow \mathbb{R}^n$ represent the logits of an L-layer fully-connected neural network where each hidden layer $h^{(l)}(x) \in \mathbb{R}^{d_l}$ is defined as follows,

$$\begin{cases} f^{(l)}(\mathbf{x}_i) = \mathbf{W}^{(l)} h^{(l-1)}(\mathbf{x}_i) \\ h^{(l)}(\mathbf{x}_i) = \sqrt{\frac{\gamma}{d_l}} \xi(f^{(l)}(\mathbf{x}_i)) \end{cases}, \quad l \in \{0, 1, \dots, L\}, \quad (1)$$

in which $\mathbf{W}^{(l)} \in \mathbb{R}^{d_l \times d_{l-1}}$ is a weight matrix drawn from $\mathcal{N}(0, \mathbf{I})$ and γ is a scaling factor to ensure that norm of each $h^{(l-1)}$ is preserved at initialization (See Du et al. (2018a) for a formal treatment). The function $\xi(\cdot)$ is also an element-wise non-linear activation function. This formulation is known as the NTK parameterization.

Let $\boldsymbol{\theta} = \text{concat}(\cup_{l=1}^L \text{vec}(\mathbf{W}^{(l)})) \in \mathbb{R}^m$ be the concatenation of all vectorized weight matrices with m as the total number of parameters.

As demonstrated by Jacot et al. (2018), in the limit of infinite width, the output of the neural network can be approximated as a linear function using a first order Taylor expansion around the initialization parameters $\boldsymbol{\theta}_0$,

$$\hat{\mathbf{y}}(\mathbf{X}, \boldsymbol{\theta}) = \hat{\mathbf{y}}_0 + \left. \frac{\partial \hat{\mathbf{y}}(\mathbf{X}, \boldsymbol{\theta})}{\partial \boldsymbol{\theta}} \right|_{\boldsymbol{\theta}_0} \boldsymbol{\theta}. \quad (2)$$

Thus, the neural network becomes a linear model as a function of the parameters while it remains a non-linear function of the inputs. The Jacobian matrix defines a feature map, which following Cao and Gu (2019), we refer to as the neural tangent random feature (NTRF) matrix,

$$\boldsymbol{\Phi}(\mathbf{X}, \boldsymbol{\theta}) = \frac{\partial \hat{\mathbf{y}}(\mathbf{X}, \boldsymbol{\theta})}{\partial \boldsymbol{\theta}} \in \mathbb{R}^{n \times m}, \quad (3)$$

$$\boldsymbol{\Phi}_0 \equiv \boldsymbol{\Phi}(\mathbf{X}, \boldsymbol{\theta}_0), \quad (4)$$

where $\boldsymbol{\Phi}_0$ is NTRF at the initialization and $\boldsymbol{\Phi}$ has shown to remain almost constant during the course of training (See for example Lee et al., 2019). The output of the neural network is then approximated,

$$\hat{\mathbf{y}}(\mathbf{X}, \boldsymbol{\theta}) = \hat{\mathbf{y}}_0 + \boldsymbol{\Phi}_0 \boldsymbol{\theta}. \quad (5)$$

We define the network's response to a training example to be the deviation from its initialization value,

$$\mathbf{r} = \mathbf{Y}(\hat{\mathbf{y}} - \hat{\mathbf{y}}_0) = \mathbf{Y}\Phi_0\boldsymbol{\theta}, \quad (6)$$

where for ease of notation we have defined $\mathbf{Y} = \text{diag}(\mathbf{y})$. A positive response implies a correct classification, while its magnitude corresponds to the network's confidence.

We are interested in characterizing the evolution of the network's response over the course of learning. Using the singular-value-decomposition (SVD) of $\mathbf{Y}\Phi_0$, we decompose the network's response along the principal components of the NTRF matrix which are the same as those of the NTK Gram matrix. Such a decomposition provides the dominant directions in the feature space and the parameter space (Yang and Salman, 2019). We, therefore, introduce the following definition.

Definition 1 (Feature). *We define a **feature** from the singular value decomposition (SVD) of the NTRF,*

$$\mathbf{Y}\Phi_0 = \mathbf{U}\mathbf{S}\mathbf{V}^T, \quad (7)$$

where $(\mathbf{V}^T)_j$ describe the j th feature, $(\mathbf{S})_{jj}$ is the strength of that feature and $(\mathbf{U})_{.j}$ contains the weights of this feature in each example adjusted according to the labels \mathbf{y} . For example, if all elements of $(\mathbf{U})_{.j}$ are positive, it translates to a perfect correlation between this feature and class labels.

Given this definition, we can define the **neural network's response to a feature** j to be the sum of the responses to each example multiplied by the weight of the feature in each example,

$$\mathbf{z} = \mathbf{U}^T \mathbf{r} = \mathbf{S}\mathbf{V}^T \boldsymbol{\theta}. \quad (8)$$

3.3 Training Dynamics

The training is performed by minimizing the following ridge-regularized cross-entropy function,

$$\mathcal{L}(\boldsymbol{\theta}) = \mathbf{1} \cdot \left(\log [1 + \exp(-\mathbf{Y}\hat{\mathbf{y}})] + \frac{\lambda}{2} \|\boldsymbol{\theta}\|^2 \right), \quad (9)$$

in which $\frac{\lambda}{2} \|\boldsymbol{\theta}\|^2$ is the weight decay regularization term. Note that the weight decay does not impose any restriction and we allow for $\lambda \in [0, \infty)$.

Direct minimization of this loss function using the gradient descent would lead to coupled dynamics and is difficult in its general form (Combes et al., 2018). As an alternative, we treat the corresponding dual optimization problem using the following variational lower bound (Jaakkola and Haussler, 1999) derived by

the Legendre transformation of the loss function. The Legendre transformation is derived according to the following inequality,

$$\log [1 + \exp (-\mathbf{Y}\hat{\mathbf{y}})] \geq H(\boldsymbol{\alpha}) - \boldsymbol{\alpha} \odot \mathbf{Y}\hat{\mathbf{y}}, \quad (10)$$

where,

$$H(\boldsymbol{\alpha}) = -[\boldsymbol{\alpha} \log \boldsymbol{\alpha} + (1 - \boldsymbol{\alpha}) \log (1 - \boldsymbol{\alpha})], \quad (11)$$

is the Shannon's binary entropy function and $\boldsymbol{\alpha} \in (0, 1)$ is a variational parameter. The equality holds when the maximum of r.h.s. with respect to $\boldsymbol{\alpha}$ is achieved at $\boldsymbol{\alpha}^* = \frac{\partial \mathcal{L}}{\partial (\mathbf{Y}\hat{\mathbf{y}})^T}$.

By treating $\boldsymbol{\theta}$ and $\boldsymbol{\alpha}$ as two free parameters, we arrive at the following optimizing problem,

$$\min_{\theta_p} \mathcal{L}(\theta_q) = \min_{\theta_p} \max_{\alpha_i} \left[\mathbf{1} \cdot \left(H(\boldsymbol{\alpha}) - \boldsymbol{\alpha} \odot \mathbf{Y}\hat{\mathbf{y}} + \frac{\lambda}{2} \|\boldsymbol{\theta}\|^2 \right) \right], \quad (12)$$

where the order of maximization and minimization can be swapped,

$$\min_{\theta_p} \mathcal{L}(\theta_q) = \max_{\alpha_i} \min_{\theta_p} \left[\mathbf{1} \cdot \left(H(\boldsymbol{\alpha}) - \boldsymbol{\alpha} \odot \mathbf{Y}\hat{\mathbf{y}} + \frac{\lambda}{2} \|\boldsymbol{\theta}\|^2 \right) \right]. \quad (13)$$

Since the neural network's output is approximated by a linear function of θ_p , the minimization can be performed analytically with an optimal value,

$$\boldsymbol{\theta}^* = \frac{1}{\lambda} \boldsymbol{\alpha} \mathbf{Y} \boldsymbol{\Phi}_0. \quad (14)$$

Now, the optimization problem amounts to the following maximization problem on the dual variable $\boldsymbol{\alpha}$,

$$\min_{\theta_p} \mathcal{L}(\theta_q) = \max_{\alpha_i} \left[H(\boldsymbol{\alpha}) - \frac{1}{2\lambda} \boldsymbol{\alpha} \mathbf{Y} \boldsymbol{\Phi}_0 \boldsymbol{\Phi}_0^T \mathbf{Y}^T \boldsymbol{\alpha}^T \right]. \quad (15)$$

By applying continuous-time gradient ascent on this optimization problem, we derive the following autonomous differential equation for the evolution of α_i ,

$$\dot{\boldsymbol{\alpha}} = \eta \left(\log \frac{(1 - \boldsymbol{\alpha})}{\boldsymbol{\alpha}} - \frac{1}{\lambda} \boldsymbol{\alpha} \mathbf{Y} \boldsymbol{\Phi}_0 \boldsymbol{\Phi}_0^T \mathbf{Y}^T \right), \quad (16)$$

where η is the learning rate. Replacing the earlier definition of the feature in Eq. 8, we get,

$$\dot{\boldsymbol{\alpha}} = \eta \left(-\log \boldsymbol{\alpha} + \log (1 - \boldsymbol{\alpha}) - \frac{1}{\lambda} \boldsymbol{\alpha} \mathbf{U} \mathbf{S}^2 \mathbf{U}^T \right). \quad (17)$$

Analyzing the qualitative properties of this dynamical system, we note that the logarithm terms act as barrier terms that keep the system within the domain $\boldsymbol{\alpha} \in (0, 1)$. The other term depends on the matrix $\mathbf{U} \mathbf{S}^2 \mathbf{U}^T$, which is positive definite. This implies that this term drives the system towards the origin and therefore drives the learning.

We can show that the learning converges towards an optimal point as $t \rightarrow \infty$.

Theorem 1. Any fixed points of the autonomous system in Eq. 17 is attractive in the domain $\alpha_i \in (0, 1)$.

At a fixed point $\boldsymbol{\alpha}^*$, the feature response of the neural network is given by

$$\mathbf{z}^* = \frac{1}{\lambda} \mathbf{S}^2 \mathbf{U}^T \boldsymbol{\alpha}^*. \quad (18)$$

In the limit of $\lambda \ll s_k^2$, where k is an index over the singular values, the linear term dominates, and the fixed point is drawn closer towards the origin. Performing a Taylor expansion around the origin, the second term in Eq. 17 can be ignored, and the dynamics are reasonably approximated as,

$$\dot{\boldsymbol{\alpha}} = \eta \left(-\log \boldsymbol{\alpha} - \frac{1}{\lambda} \boldsymbol{\alpha} \mathbf{U} (\mathbf{S}^2 + \lambda \mathbf{I}) \mathbf{U}^T \right). \quad (19)$$

3.4 Gradient Starvation

In general, we do not expect to find an analytical solution for the dynamics of this coupled non-linear dynamical system. However, there are at least two cases where a decoupled form for the dynamics allows to find an exact solution. We first introduce these cases and then study their perturbation.

1. If the matrix of singular values \mathbf{S}^2 is proportional to the identity: This is the case where all the features have the same strength s^2 . The fixed points are then given by,

$$\begin{aligned} \alpha_i^* &= \frac{\lambda \mathcal{W}(\lambda^{-1} s^2 + \lambda)}{s^2 + \lambda}, \\ z_j^* &= \frac{s^2 \mathcal{W}(\lambda^{-1} s^2 + 1)}{s^2 + \lambda} \sum_i u_{ij}, \end{aligned} \quad (20)$$

where \mathcal{W} is the Lambert W function.

2. If the matrix \mathbf{U} is a permutation matrix: This is the case in which each feature is associated with a single example only. The fixed points are then given by,

$$\begin{aligned} \alpha_i^* &= \frac{\lambda \mathcal{W}(\lambda^{-1} s_i^2 + 1)}{s_i^2 + \lambda}, \\ z_j^* &= \frac{s_i^2 \mathcal{W}(\lambda^{-1} s_i^2 + 1)}{s_i^2 + \lambda}. \end{aligned} \quad (21)$$

To study a minimal case of starvation, we consider a variation of case 2 with the following assumption.

Assumption 1. Assume \mathbf{U} is a matrix in which the off-diagonal elements are proportional to a small parameter $\delta > 0$.

Lemma 1. Under assumption 1, the fixed point of the dynamical system in Eq. 17 can be approximated by,

$$\tilde{\boldsymbol{\alpha}}^* = (1 - \log(\boldsymbol{\alpha}^*)) \left[\mathbf{A} + \text{diag}(\boldsymbol{\alpha}^{*-1}) \right]^{-1}, \quad (22)$$

where $\mathbf{A} = \lambda^{-1} \mathbf{U} (\mathbf{S}^2 + \lambda \mathbf{I}) \mathbf{U}^T$.

Since treating a general \mathbf{U} is significantly more complicated, we restrict ourselves to a two dimensional case where,

$$\mathbf{U} = \begin{pmatrix} \sqrt{1-\delta^2} & -\delta \\ \delta & \sqrt{1-\delta^2} \end{pmatrix}. \quad (23)$$

Theorem 2 (Gradient Starvation). Suppose a neural network in the linear regime, trained under cross-entropy loss for a binary classification task. With definition 1, assuming coupling between features 1 and 2 as in Eq. 23 and $s_1^2 > s_2^2$, we have,

$$\frac{d\tilde{z}_2^*}{ds_1^2} < 0, \quad (24)$$

which implies that an increase in the strength of feature 1 has a detrimental effect on the learning of feature 2.

3.5 Spectral Decoupling

Thm. 2 results from the coupling between the features during the course of learning. A solution to counteract it would be to decouple the dynamics. We propose Spectral Decoupling (SD) and prove that the dynamics decouple by simply replacing the weight decay term with an L2 penalty on the network's logits,

$$\mathcal{L}(\boldsymbol{\theta}) = \mathbf{1} \cdot \left(\log [1 + \exp(-\mathbf{Y}\hat{\mathbf{y}})] + \frac{\lambda}{2} \|\hat{\mathbf{y}}\|^2 \right). \quad (25)$$

In this case, the dual optimization problem takes the form,

$$\mathcal{L}(\boldsymbol{\theta}) = \max_{\alpha_i} \mathbf{1} \cdot \left(H(\boldsymbol{\alpha}) - \frac{1}{2\lambda} \boldsymbol{\alpha} \boldsymbol{\alpha}^T \right), \quad (26)$$

and the dynamics of the dual parameters is described by,

$$\dot{\boldsymbol{\alpha}} = \eta \left(-\log \boldsymbol{\alpha} + \log(\mathbf{1} - \boldsymbol{\alpha}) - \frac{1}{\lambda} \boldsymbol{\alpha} \right), \quad (27)$$

which is indeed an uncoupled autonomous system in which no gradient starvation effect is manifested.

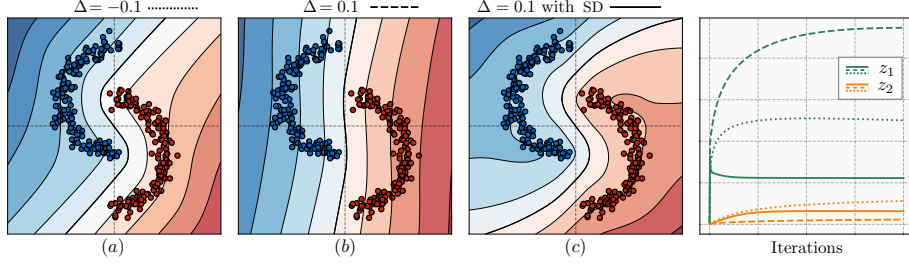


Fig. 2: (a) shows the learned decision boundary for an arrangement of the datapoints where the two classes are not linearly separable ($\Delta < 0$). (b) on linearly separable data ($\Delta > 0$), the learned decision boundary is almost linear. (c) on the same linearly separable data, spectral decoupling learns a curved decision boundary with a larger margin. (Right) shows the evolution of two of the feature (Eq. 8) of the dynamics in (a), (b) and (c) shown as dotted, dashed and solid lines respectively. (a) vs (b): Linear separability of the data results in an increase in z_1 and a decrease (starvation) in z_2 . (b) vs (c): Spectral Decoupling (SD) suppresses z_1 and hence allows z_2 to grow. Decision boundaries are average over 10 runs.

4 Experiments

In this section, we conduct several experiments on both toy and real-world tasks. The experiments presented here are designed to pinpoint the existence of GS and its consequences, as well as the efficacy of our proposed regularization method to alleviate them. Consequently, we highlight that achieving state-of-the-art results is not the objective. Nevertheless, it appears that our proposed Spectral Decoupling achieves state-of-the-art results in some cases. Details on the experiments and learning recipes are provided in App. A.

Two-Moon Classification. Consider a simple 2-dimensional classification task between red and blue data points in Figure. 2. We use a two layer ($L = 3$) neural network with 500 hidden units and with *ReLU* non-linearity. We train the network on different arrangements of the data points and visualize the learned decision boundary. Arrangements differ in the linear separability of the two classes denoted by Δ . A $\Delta < 0$ means that the two classes are not linearly separable while $\Delta > 0$ means that the classes are linearly separable.

In Figure. 2, the plots (a-c) demonstrate the learned decision boundary. The only difference between (a) and (b) is that in (b), the two classes are linearly separable with a small margin. This subtle difference leads to a very sharp (high Lipschitz) and linear decision boundary located very close to the data points. The right plot shows that the linear separability results in *starvation* of the second feature. (c) illustrates the effect of using the proposed spectral decoupling (SD) on the learned decision boundary. While in (b), the learned decision boundary can only discriminate along the x-axis, spectral decoupling leads to learning of a curved decision boundary with a larger margin in the

input space. It should be stressed that our proposed spectral decoupling does not explicitly aim at maximizing the margin and the observed improvement is a by-product of decoupled learning of features. See Section 5 to discuss why cross-entropy results in a poor margin while being considered a max-margin classifier in the literature. (Soudry et al., 2018).

Colored MNIST with color bias. We conduct experiments on the Colored MNIST Dataset, proposed in Arjovsky et al. (2019). The task is to predict binary labels $y = -1$ for digits 0 to 4 and $y = +1$ for digits 5 to 9. A color channel is artificially added to each example to deliberately impose a spurious correlation between the color and the label. However, an opposite correlation between the color and the label is present in the test set. Also, a 25 % label noise is added to both the training and test datasets, and hence an oracle that totally ignores the color should get ~75 % accuracy, as shown in Table 1. Empirical Risk Minimization (ERM - vanilla cross-entropy) performs well on the training set (91.1 %) but poorly on the test set (23.9 %). It is expected because the color feature is reversed in the test set, and we cannot expect the model to ignore the color. On the other hand, Invariant Risk Minimization (IRM) achieves good performance on the test set (67.1 %). However, SD also performs well (68.4 %) without requiring access to multiple training environments, unlike IRM.

A natural question that arises is how SD is ignoring the color feature without having access to multiple environments? The answer is that SD does not ignore the color and indeed learns it. However, SD **also** learns other predictive features, i.e., the digits' shape. It appears that at the test time, the predictions resulting from the shape features prevail over the color feature. See Appendix B for more details.

We should highlight that, by design, this task assumes access to the test for hyperparameter tuning for all the reported methods. This is not a valid assumption in general, and hence the results should be interpreted only as a probe that shows that SD provides an important level of control over what features are learned.

Method	Train Accuracy	Test Accuracy
ERM (Vanilla Cross-Entropy)	91.1 % (± 0.4)	23.7 % (± 0.8)
REx (Krueger et al., 2020)	71.5 % (± 1.0)	68.7 % (± 0.9)
IRM (Arjovsky et al., 2019)	70.5 % (± 0.6)	67.1 % (± 1.4)
SD (this work)	70.0 % (± 0.9)	68.4 % (± 1.2)
Oracle - trained on grayscale images	73.5 % (± 0.2)	73.0 % (± 0.4)
Random Guess		50 %

Table 1: Test accuracy on test examples of the Colored MNIST after training for 1k epochs. The standard deviation over 10 runs is reported in parenthesis. ERM stands for the empirical risk minimization. Oracle is an ERM on grayscale images. Note that due to label noise, a hypothetical optimum achieves 75 % accuracy.

Method	Worst Group Accuracy	Average Accuracy
ERM	40.35 % (± 1.68)	94.61 % (± 0.67)
SD (this work)	83.24 % (± 2.01)	91.64 % (± 0.61)
LfF (Nam et al., 2020)	81.24 % (± 1.38)	n/a
Group DRO* (Sagawa et al., 2019)	87.78 % (± 0.96)	91.76 % (± 0.28)

Table 2: Results on the held-out test set of CelebA. The task is to classify images into two classes of `blond` or `dark` hair. However, the `HairColor` and the `Gender` are spuriously correlated where only 0.85 % of the training set are `blond males`. This spurious correlation leads to poor OOD generalization performance when trained with vanilla cross-entropy loss, but spectral decoupling significantly improves performance.
*Group DRO requires explicit information about the spurious correlation. The standard deviation over ten runs is reported in parenthesis.

CelebA with gender bias. The CelebA dataset (Liu et al., 2015) contains 162k celebrity faces with binary attributes associated with each image. Following the setup of (Sagawa et al., 2019), the task is to classify images with respect to their hair color into two classes of blond or dark hair. However, the `Gender` $\in \{\text{Male, Female}\}$ is spuriously correlated with the `HairColor` $\in \{\text{Blond, Dark}\}$ in the training data. The rarest group which is blond males builds only 0.85 % of the training data (1387 out of 162k examples).

We train a ResNet-50 model (He et al., 2016) on this task. Table 2 summarizes the results and compares the performance of several methods. We choose the model with the best validation accuracy during training and for hyper-parameter search and report the results on a held-out test set. A model with the vanilla cross-entropy appears to generalize well on average but fails to generalize to the rarest group (blond male) which can be considered as out-of-distribution (OOD). On the other hand, our proposed spectral decoupling improves the performance more than double. It should be highlighted that for this task, we use a variant of spectral decoupling in which,

$$\frac{\lambda}{2} \|\hat{y} - \gamma\|_2^2, \quad (28)$$

is added to the original cross-entropy loss. The hyper-parameters λ and γ are tuned separately for each class (a total of four hyper-parameters). This variant of SD does provably decouple the dynamics but appears to perform better than the original SD in Eq. 25 in this task.

Other proposed methods presented in Table 2 also improve the performance of the worst group significantly. The recently proposed "Learning from failure" (LfF) (Nam et al., 2020) achieves comparable results to spectral decoupling, but it requires simultaneous training of two networks. One network distinguishes the bias, and the other uses the first network to "debias" the learning. Group DRO (Sagawa et al., 2019) is another successful method for this task. However, unlike spectral decoupling, Group DRO requires explicit information about the

spuriously correlated attributes. In most practical tasks, information about the spurious correlations is not provided and in many cases, dependence on the spurious correlation goes unrecognized. Recall that it took three years for the psychologist, Oskar Pfungst, to realize that Clever Hans was not capable of doing any arithmetic.

5 Related Work and Discussion

On learning dynamics. Baldi and Hornik (1989), Heskes and Kappen (1993), and Le Cun et al. (1991) are among early works that study the dynamics of gradient descent in continuous time. More recently, Saxe et al. (2013, 2019); Advani and Saxe (2017); Lampinen and Ganguli (2018) investigate the dynamics of deep linear networks trained with squared-error loss and derive analytical solutions despite the non-linearity of the dynamics. The message is that the training process can be decomposed into independent learning dynamics along the orthogonal directions (modes) of the input covariance matrix. The corresponding eigenvalue determines the speed of learning along each mode. In these cases, no gradient starvation happens as the result of the so-called “independent mode learning”. Thanks to the introduction of the *neural tangent kernel* (NTK) (Jacot et al., 2018), several works were able to extend the study of learning dynamics to non-linear, wide, and over-parameterized neural networks, as reviewed in Section 3.1. However, most of the work in this area focuses on square-error loss which for linear networks, leads to decoupled learning dynamics. In this work, our focus was the cross-entropy loss, an objective commonly used in practice.

On reliance upon spurious correlations and robustness. In the context of robustness in neural networks, state-of-the-art neural networks appear to naturally focus on low-level superficial correlations rather than more abstract and robustly informative features of interest (e.g. Geirhos et al. (2020)). As we argue in this work, Gradient Starvation is likely an important factor contributing to this phenomenon and can result in adversarial vulnerability. There is a rich research literature on adversarial attacks and neural networks’ vulnerability (Szegedy et al., 2013; Goodfellow et al., 2014; Ilyas et al., 2019; Madry et al., 2017; Akhtar and Mian, 2018; Ilyas et al., 2018). Interestingly, Nar and Sastry (2019), Nar et al. (2019) and Jacobsen et al. (2018) draw a similar conclusion and argue that “an insufficiency of the cross-entropy loss” causes excessive invariances to predictive features. Perhaps Shah et al. (2020) is the closest to our work in which authors study the simplicity bias (SB) in stochastic gradient descent. They demonstrate that neural networks exhibit extreme bias that could lead to adversarial vulnerability.

On implicit bias. Modern neural networks generalize surprisingly well in numerous machine tasks. This is despite the fact that neural networks typically contain orders of magnitude more parameters than the number of examples in

a training set and have sufficient capacity to fit a totally randomized dataset perfectly (Zhang et al., 2016). The widespread explanation is that the gradient descent has a form of implicit bias towards learning simpler functions that generalize better according to Occam’s razor. Our view of Gradient Starvation reinforces this explanation. In essence, when training and test data points are drawn from the same distribution, the top salient features are predictive in both sets. We conjecture that in such a scenario, by not learning the less salient features, Gradient Starvation naturally protects the network from overfitting. The same phenomenon is referred to as *implicit bias*, *implicit regularization*, *simplicity bias* and *spectral bias* in several works (Rahaman et al., 2019; Neyshabur et al., 2014; Gunasekar et al., 2017; Neyshabur et al., 2017; Nakkiran et al., 2019; Ji and Telgarsky, 2019; Soudry et al., 2018; Arora et al., 2019a; Arpit et al., 2017; Gunasekar et al., 2018; Poggio et al., 2017; Ma et al., 2018). As an active line of research, numerous studies have provided different explanations for this phenomenon. For example, Nakkiran et al. (2019) justifies the implicit bias of neural networks by showing that stochastic gradient descent learns simpler functions first. Baratin et al. (2020); Oymak et al. (2019) suggests that a form of implicit regularization is induced by an alignment between NTK’s principal components and only a few task-relevant directions. Several other works such as Brutzkus et al. (2017); Gunasekar et al. (2018); Soudry et al. (2018); Chizat and Bach (2018) recognize the convergence of gradient descent to maximum-margin solution as the essential factor for the generalizability of neural networks. It should be stressed that these work refer to the margin in the hidden space and not in the input space as pointed out in Jolicoeur-Martineau and Mitliagkas (2019). Indeed, as observed in our experiments, the maximum-margin classifier in the hidden space can be achieved at the expense of a small margin in the input space.

On Gradient Starvation and no free lunch theorem. The *no free lunch* theorem (Shalev-Shwartz and Ben-David, 2014; Wolpert, 1996) states that “learning is impossible without making assumptions about training and test distributions”. Probably, the most commonly used assumption of machine learning is the i.i.d. assumption (Vapnik and Vapnik, 1998), which assumes that both training and test data are identically distributed. However, in general, this assumption might not hold, and in many practical applications, there are predictive features in the training set that do not generalize to the test set.

Now the question is *how to favor generalizable features over spurious features?* The most common approaches include *data augmentation*, *controlling the inductive biases*, *using regularizations*, and more recently *training using multiple environments*.

Here, we would like to elaborate on an interesting thought experiment of Parascandolo et al. (2020): Suppose a neural network is provided with a chess book containing examples of chess boards with the best movement indicated by a red arrow. The network can take two approaches: 1) To learn how to play chess, or 2) To learn just the red arrows. Either of these solutions results in zero training

loss while only the former is generalizable. With no external knowledge or any inductive biases, the network learns the simpler solution which is to memorize the red arrows.

Recent works such as (Arjovsky et al., 2019; Krueger et al., 2020; Parascandolo et al., 2020; Ahuja et al., 2020a) assume that the network has also access to another chess book in which blue writings indicate the best movement. They each introduce novel methods to aggregate information from multiple training environments in a way that favors the generalizable / domain-agnostic / invariant solution.

In this paper, we argue that even with having access to **only one** training environment, there is useful information in the training set that fails to be discovered due to Gradient Starvation. The information on how to actually play chess is already available in any of the chess books. Still, as soon as the network learns the red arrows, the network has no incentive for further learning because of Gradient Starvation. Therefore, learning the red arrows is not an issue per se, but not learning to play chess is.

A better understanding and control of Gradient Starvation and its impact on generalization offers promising avenues to address this issue with minimal assumptions. Indeed, our Spectral Decoupling method requires an assumption about feature imbalance but not to pinpoint them exactly, relying on modulated learning dynamics to achieve balance.

6 Conclusion

In this paper, we formalized gradient starvation as a phenomenon that emerges when training with cross-entropy loss in neural networks. By analyzing the dynamical system corresponding to the learning process in dual space, we showed that gradient starvation could slow down the learning of certain features, even if they are present in the training set. This phenomenon can have both adverse and beneficial consequences. If the learned features are sufficient to generalize to the test data, gradient starvation can be viewed as an implicit regularizer. Otherwise, gradient starvation could have an unfavorable effect, which we observe empirically when some predictive features fail to be learned. We also derived spectral decoupling regularization as a possible remedy to gradient starvation. We hope that our analyses pave the path towards a better understanding of neural networks' learning.

Acknowledgments

We gratefully acknowledge the support of Google DeepMind and CIFAR. This research was enabled in part by support provided by [Calcul Quebec](#) and [Compute Canada](#). We would like to express our appreciation to Reyhane Askari Hemmat, Faruk Ahmed, Aristide Baratin, Ethan Caballero, Kostiantyn Lapchevskyi, Philemon Brakel, Philippe Hamel, Shibl Mourad, Charan Reddy, Arna Ghosh for their valuable and constructive suggestions and discussions. We would also

like to thank Çağlar Gülcöhre, Razvan Pascanu, Alex Graves, Sasha Vezhnevets, James Martens, Hossein Askari Hemmat, Madhu Advani, Rémi Le Priol, Ankesh Anand and Zac Kenton for their feedback.

Bibliography

- Advani, M. S. and Saxe, A. M. (2017). High-dimensional dynamics of generalization error in neural networks. *arXiv preprint arXiv:1710.03667*.
- Advani, M. S., Saxe, A. M., and Sompolinsky, H. (2020). High-dimensional dynamics of generalization error in neural networks. *Neural Networks*.
- Ahuja, K., Shanmugam, K., and Dhurandhar, A. (2020a). Linear regression games: Convergence guarantees to approximate out-of-distribution solutions. *arXiv preprint arXiv:2010.15234*.
- Ahuja, K., Shanmugam, K., Varshney, K., and Dhurandhar, A. (2020b). Invariant risk minimization games. *arXiv preprint arXiv:2002.04692*.
- Akhtar, N. and Mian, A. (2018). Threat of adversarial attacks on deep learning in computer vision: A survey. *IEEE Access*, 6:14410–14430.
- Allen-Zhu, Z., Li, Y., and Liang, Y. (2019a). Learning and generalization in overparameterized neural networks, going beyond two layers. In *Advances in neural information processing systems*, pages 6158–6169.
- Allen-Zhu, Z., Li, Y., and Song, Z. (2019b). A convergence theory for deep learning via over-parameterization. In *International Conference on Machine Learning*, pages 242–252. PMLR.
- Arjovsky, M., Bottou, L., Gulrajani, I., and Lopez-Paz, D. (2019). Invariant risk minimization. *arXiv preprint arXiv:1907.02893*.
- Arora, S., Cohen, N., Hu, W., and Luo, Y. (2019a). Implicit regularization in deep matrix factorization. In *Advances in Neural Information Processing Systems*, pages 7413–7424.
- Arora, S., Du, S. S., Hu, W., Li, Z., Salakhutdinov, R. R., and Wang, R. (2019b). On exact computation with an infinitely wide neural net. In *Advances in Neural Information Processing Systems*, pages 8139–8148.
- Arora, S., Du, S. S., Hu, W., Li, Z., and Wang, R. (2019c). Fine-grained analysis of optimization and generalization for overparameterized two-layer neural networks. *arXiv preprint arXiv:1901.08584*.
- Arpit, D., Jastrzębski, S., Ballas, N., Krueger, D., Bengio, E., Kanwal, M. S., Maharaj, T., Fischer, A., Courville, A., Bengio, Y., et al. (2017). A closer look at memorization in deep networks. *arXiv preprint arXiv:1706.05394*.
- Baker, N., Lu, H., Erlikhman, G., and Kellman, P. J. (2018). Deep convolutional networks do not classify based on global object shape. *PLoS computational biology*, 14(12):e1006613.
- Baldi, P. and Hornik, K. (1989). Neural networks and principal component analysis: Learning from examples without local minima. *Neural networks*, 2(1):53–58.
- Baratin, A., George, T., Laurent, C., Hjelm, R. D., Lajoie, G., Vincent, P., and Lacoste-Julien, S. (2020). Implicit regularization in deep learning: A view from function space. *arXiv preprint arXiv:2008.00938*.
- Beery, S., Van Horn, G., and Perona, P. (2018). Recognition in terra incognita. In *Proceedings of the European Conference on Computer Vision (ECCV)*, pages 456–473.
- Belinkov, Y. and Bisk, Y. (2017). Synthetic and natural noise both break neural machine translation. *arXiv preprint arXiv:1711.02173*.
- Bietti, A. and Mairal, J. (2019). On the inductive bias of neural tangent kernels. In *Advances in Neural Information Processing Systems*, pages 12893–12904.

- Brendel, W. and Bethge, M. (2019). Approximating cnns with bag-of-local-features models works surprisingly well on imagenet. *arXiv preprint arXiv:1904.00760*.
- Brutzkus, A., Globerson, A., Malach, E., and Shalev-Shwartz, S. (2017). Sgd learns over-parameterized networks that provably generalize on linearly separable data. *arXiv preprint arXiv:1710.10174*.
- Cao, Y., Fang, Z., Wu, Y., Zhou, D.-X., and Gu, Q. (2019). Towards understanding the spectral bias of deep learning. *arXiv preprint arXiv:1912.01198*.
- Cao, Y. and Gu, Q. (2019). Generalization bounds of stochastic gradient descent for wide and deep neural networks. In *Advances in Neural Information Processing Systems*, pages 10836–10846.
- Chizat, L. and Bach, F. (2018). A note on lazy training in supervised differentiable programming. *arXiv preprint arXiv:1812.07956*, 1.
- Combes, R. T. d., Pezeshki, M., Shabanian, S., Courville, A., and Bengio, Y. (2018). On the learning dynamics of deep neural networks. *arXiv preprint arXiv:1809.06848*.
- Du, S. S., Hu, W., and Lee, J. D. (2018a). Algorithmic regularization in learning deep homogeneous models: Layers are automatically balanced. In *Advances in Neural Information Processing Systems*, pages 384–395.
- Du, S. S., Zhai, X., Poczos, B., and Singh, A. (2018b). Gradient descent provably optimizes over-parameterized neural networks. *arXiv preprint arXiv:1810.02054*.
- Geirhos, R., Jacobsen, J.-H., Michaelis, C., Zemel, R., Brendel, W., Bethge, M., and Wichmann, F. A. (2020). Shortcut learning in deep neural networks. *arXiv preprint arXiv:2004.07780*.
- George, T. (2020). Nngeometry: Easy and fast fisher information matrices and neural tangent kernels in pytorch.
- Gidel, G., Bach, F., and Lacoste-Julien, S. (2019). Implicit regularization of discrete gradient dynamics in linear neural networks. In *Advances in Neural Information Processing Systems*, pages 3202–3211.
- Goldt, S., Advani, M., Saxe, A. M., Krzakala, F., and Zdeborová, L. (2019). Dynamics of stochastic gradient descent for two-layer neural networks in the teacher-student setup. In *Advances in Neural Information Processing Systems*, pages 6981–6991.
- Goodfellow, I. J., Shlens, J., and Szegedy, C. (2014). Explaining and harnessing adversarial examples. *arXiv preprint arXiv:1412.6572*.
- Gunasekar, S., Lee, J. D., Soudry, D., and Srebro, N. (2018). Implicit bias of gradient descent on linear convolutional networks. In *Advances in Neural Information Processing Systems*, pages 9461–9471.
- Gunasekar, S., Woodworth, B. E., Bhojanapalli, S., Neyshabur, B., and Srebro, N. (2017). Implicit regularization in matrix factorization. In *Advances in Neural Information Processing Systems*, pages 6151–6159.
- Gururangan, S., Swayamdipta, S., Levy, O., Schwartz, R., Bowman, S. R., and Smith, N. A. (2018). Annotation artifacts in natural language inference data. *arXiv preprint arXiv:1803.02324*.
- He, K., Zhang, X., Ren, S., and Sun, J. (2016). Deep residual learning for image recognition. In *Proceedings of the IEEE conference on computer vision and pattern recognition*, pages 770–778.
- Heinze-Deml, C. and Meinshausen, N. (2017). Conditional variance penalties and domain shift robustness. *arXiv preprint arXiv:1710.11469*.
- Hendrycks, D. and Dietterich, T. (2019). Benchmarking neural network robustness to common corruptions and perturbations. *arXiv preprint arXiv:1903.12261*.
- Hendrycks, D. and Gimpel, K. (2016). A baseline for detecting misclassified and out-of-distribution examples in neural networks. *arXiv preprint arXiv:1610.02136*.

- Hermann, K. L. and Lampinen, A. K. (2020). What shapes feature representations? exploring datasets, architectures, and training. *arXiv preprint arXiv:2006.12433*.
- Heskes, T. M. and Kappen, B. (1993). On-line learning processes in artificial neural networks. In *North-Holland Mathematical Library*, volume 51, pages 199–233. Elsevier.
- Huang, J. and Yau, H.-T. (2019). Dynamics of deep neural networks and neural tangent hierarchy. *arXiv preprint arXiv:1909.08156*.
- Ilyas, A., Engstrom, L., Athalye, A., and Lin, J. (2018). Black-box adversarial attacks with limited queries and information. *arXiv preprint arXiv:1804.08598*.
- Ilyas, A., Santurkar, S., Tsipras, D., Engstrom, L., Tran, B., and Madry, A. (2019). Adversarial examples are not bugs, they are features. In *Advances in Neural Information Processing Systems*, pages 125–136.
- Ioffe, S. and Szegedy, C. (2015). Batch normalization: Accelerating deep network training by reducing internal covariate shift. *arXiv preprint arXiv:1502.03167*.
- Jaakkola, T. S. and Haussler, D. (1999). Probabilistic kernel regression models. In *AISTATS*.
- Jacobsen, J.-H., Behrmann, J., Zemel, R., and Bethge, M. (2018). Excessive invariance causes adversarial vulnerability. *arXiv preprint arXiv:1811.00401*.
- Jacot, A., Gabriel, F., and Hongler, C. (2018). Neural tangent kernel: Convergence and generalization in neural networks. In *Advances in neural information processing systems*, pages 8571–8580.
- Ji, Z. and Telgarsky, M. (2019). The implicit bias of gradient descent on nonseparable data. In *Conference on Learning Theory*, pages 1772–1798.
- Jo, J. and Bengio, Y. (2017). Measuring the tendency of cnns to learn surface statistical regularities. *arXiv preprint arXiv:1711.11561*.
- Jolicoeur-Martineau, A. and Mitliagkas, I. (2019). Connections between support vector machines, wasserstein distance and gradient-penalty gans. *arXiv preprint arXiv:1910.06922*.
- Kingma, D. P. and Ba, J. (2014). Adam: A method for stochastic optimization. *arXiv preprint arXiv:1412.6980*.
- Krogh, A. and Hertz, J. A. (1992). A simple weight decay can improve generalization. In *Advances in neural information processing systems*, pages 950–957.
- Krueger, D., Caballero, E., Jacobsen, J.-H., Zhang, A., Binns, J., Priol, R. L., and Courville, A. (2020). Out-of-distribution generalization via risk extrapolation (rex). *arXiv preprint arXiv:2003.00688*.
- Lampinen, A. K. and Ganguli, S. (2018). An analytic theory of generalization dynamics and transfer learning in deep linear networks. *arXiv preprint arXiv:1809.10374*.
- Lapuschkin, S., Wäldchen, S., Binder, A., Montavon, G., Samek, W., and Müller, K.-R. (2019). Unmasking clever hans predictors and assessing what machines really learn. *Nature communications*, 10(1):1–8.
- Le Cun, Y., Kanter, I., and Solla, S. A. (1991). Eigenvalues of covariance matrices: Application to neural-network learning. *Physical Review Letters*, 66(18):2396.
- Lee, J., Xiao, L., Schoenholz, S., Bahri, Y., Novak, R., Sohl-Dickstein, J., and Pennington, J. (2019). Wide neural networks of any depth evolve as linear models under gradient descent. In *Advances in neural information processing systems*, pages 8570–8581.
- Lee, K., Lee, K., Lee, H., and Shin, J. (2018). A simple unified framework for detecting out-of-distribution samples and adversarial attacks. In *Advances in Neural Information Processing Systems*, pages 7167–7177.
- Liang, S., Li, Y., and Srikant, R. (2017). Enhancing the reliability of out-of-distribution image detection in neural networks. *arXiv preprint arXiv:1706.02690*.
- Liu, Z., Luo, P., Wang, X., and Tang, X. (2015). Deep learning face attributes in the wild. In *Proceedings of International Conference on Computer Vision (ICCV)*.

- Ma, C., Wang, K., Chi, Y., and Chen, Y. (2018). Implicit regularization in nonconvex statistical estimation: Gradient descent converges linearly for phase retrieval and matrix completion. In *International Conference on Machine Learning*, pages 3345–3354. PMLR.
- Madry, A., Makelov, A., Schmidt, L., Tsipras, D., and Vladu, A. (2017). Towards deep learning models resistant to adversarial attacks. *arXiv preprint arXiv:1706.06083*.
- McCoy, R. T., Pavlick, E., and Linzen, T. (2019). Right for the wrong reasons: Diagnosing syntactic heuristics in natural language inference. *arXiv preprint arXiv:1902.01007*.
- Mei, S. and Montanari, A. (2019). The generalization error of random features regression: Precise asymptotics and double descent curve. *arXiv preprint arXiv:1908.05355*.
- Nakkiran, P., Kaplun, G., Kalimeris, D., Yang, T., Edelman, B. L., Zhang, F., and Barak, B. (2019). Sgd on neural networks learns functions of increasing complexity. *arXiv preprint arXiv:1905.11604*.
- Nam, J., Cha, H., Ahn, S., Lee, J., and Shin, J. (2020). Learning from failure: Training debiased classifier from biased classifier. *arXiv preprint arXiv:2007.02561*.
- Nar, K., Ocal, O., Sastry, S. S., and Ramchandran, K. (2019). Cross-entropy loss and low-rank features have responsibility for adversarial examples. *arXiv preprint arXiv:1901.08360*.
- Nar, K. and Sastry, S. S. (2019). Persistency of excitation for robustness of neural networks. *arXiv preprint arXiv:1911.01043*.
- Neyshabur, B., Tomioka, R., Salakhutdinov, R., and Srebro, N. (2017). Geometry of optimization and implicit regularization in deep learning. *arXiv preprint arXiv:1705.03071*.
- Neyshabur, B., Tomioka, R., and Srebro, N. (2014). In search of the real inductive bias: On the role of implicit regularization in deep learning. *arXiv preprint arXiv:1412.6614*.
- Niven, T. and Kao, H.-Y. (2019). Probing neural network comprehension of natural language arguments. *arXiv preprint arXiv:1907.07355*.
- Oakden-Rayner, L., Dunnmon, J., Carneiro, G., and Ré, C. (2020). Hidden stratification causes clinically meaningful failures in machine learning for medical imaging. In *Proceedings of the ACM Conference on Health, Inference, and Learning*, pages 151–159.
- Oymak, S., Fabian, Z., Li, M., and Soltanolkotabi, M. (2019). Generalization guarantees for neural networks via harnessing the low-rank structure of the jacobian. *arXiv preprint arXiv:1906.05392*.
- Parascandolo, G., Neitz, A., Orvieto, A., Gresele, L., and Schölkopf, B. (2020). Learning explanations that are hard to vary. *arXiv preprint arXiv:2009.00329*.
- Paszke, A., Gross, S., Chintala, S., Chanan, G., Yang, E., DeVito, Z., Lin, Z., Desmaison, A., Antiga, L., and Lerer, A. (2017). Automatic differentiation in pytorch.
- Pfungst, O. (1911). *Clever Hans:(the horse of Mr. Von Osten.) a contribution to experimental animal and human psychology*. Holt, Rinehart and Winston.
- Poggio, T., Kawaguchi, K., Liao, Q., Miranda, B., Rosasco, L., Boix, X., Hidary, J., and Mhaskar, H. (2017). Theory of deep learning iii: explaining the non-overfitting puzzle. *arXiv preprint arXiv:1801.00173*.
- Rahaman, N., Baratin, A., Arpit, D., Draxler, F., Lin, M., Hamprecht, F., Bengio, Y., and Courville, A. (2019). On the spectral bias of neural networks. In *International Conference on Machine Learning*, pages 5301–5310. PMLR.
- Ribeiro, M. T., Singh, S., and Guestrin, C. (2016). " why should i trust you?" explaining the predictions of any classifier. In *Proceedings of the 22nd ACM SIGKDD international conference on knowledge discovery and data mining*, pages 1135–1144.

- Ronen, B., Jacobs, D., Kasten, Y., and Kritchman, S. (2019). The convergence rate of neural networks for learned functions of different frequencies. In *Advances in Neural Information Processing Systems*, pages 4761–4771.
- Rosenfeld, A., Zemel, R., and Tsotsos, J. K. (2018). The elephant in the room. *arXiv preprint arXiv:1808.03305*.
- Sagawa, S., Koh, P. W., Hashimoto, T. B., and Liang, P. (2019). Distributionally robust neural networks for group shifts: On the importance of regularization for worst-case generalization. *arXiv preprint arXiv:1911.08731*.
- Saxe, A. M., McClelland, J. L., and Ganguli, S. (2013). Exact solutions to the nonlinear dynamics of learning in deep linear neural networks. *arXiv preprint arXiv:1312.6120*.
- Saxe, A. M., McClelland, J. L., and Ganguli, S. (2019). A mathematical theory of semantic development in deep neural networks. *Proceedings of the National Academy of Sciences*, 116(23):11537–11546.
- Shah, H., Tamuly, K., Raghunathan, A., Jain, P., and Netrapalli, P. (2020). The pitfalls of simplicity bias in neural networks. *arXiv preprint arXiv:2006.07710*.
- Shalev-Shwartz, S. and Ben-David, S. (2014). *Understanding machine learning: From theory to algorithms*. Cambridge university press.
- Soudry, D., Hoffer, E., Nacson, M. S., Gunasekar, S., and Srebro, N. (2018). The implicit bias of gradient descent on separable data. *The Journal of Machine Learning Research*, 19(1):2822–2878.
- Srivastava, N., Hinton, G., Krizhevsky, A., Sutskever, I., and Salakhutdinov, R. (2014). Dropout: a simple way to prevent neural networks from overfitting. *The journal of machine learning research*, 15(1):1929–1958.
- Szegedy, C., Zaremba, W., Sutskever, I., Bruna, J., Erhan, D., Goodfellow, I., and Fergus, R. (2013). Intriguing properties of neural networks. *arXiv preprint arXiv:1312.6199*.
- Valle-Pérez, G., Camargo, C. Q., and Louis, A. A. (2018). Deep learning generalizes because the parameter-function map is biased towards simple functions. *arXiv preprint arXiv:1805.08522*.
- Vapnik, V. and Vapnik, V. (1998). Statistical learning theory wiley. *New York*, pages 156–160.
- Vempala, S. and Wilmes, J. (2019). Gradient descent for one-hidden-layer neural networks: Polynomial convergence and sq lower bounds. In *Conference on Learning Theory*, pages 3115–3117.
- Wang, H., He, Z., Lipton, Z. C., and Xing, E. P. (2019). Learning robust representations by projecting superficial statistics out. *arXiv preprint arXiv:1903.06256*.
- Wolpert, D. H. (1996). The lack of a priori distinctions between learning algorithms. *Neural computation*, 8(7):1341–1390.
- Xu, Z.-Q. J., Zhang, Y., Luo, T., Xiao, Y., and Ma, Z. (2019a). Frequency principle: Fourier analysis sheds light on deep neural networks. *arXiv preprint arXiv:1901.06523*.
- Xu, Z.-Q. J., Zhang, Y., and Xiao, Y. (2019b). Training behavior of deep neural network in frequency domain. In *International Conference on Neural Information Processing*, pages 264–274. Springer.
- Yang, G. and Salman, H. (2019). A fine-grained spectral perspective on neural networks. *arXiv preprint arXiv:1907.10599*.
- Zech, J. R., Badgeley, M. A., Liu, M., Costa, A. B., Titano, J. J., and Oermann, E. K. (2018). Confounding variables can degrade generalization performance of radiological deep learning models. *arXiv preprint arXiv:1807.00431*.
- Zhang, C., Bengio, S., Hardt, M., Recht, B., and Vinyals, O. (2016). Understanding deep learning requires rethinking generalization. *arXiv preprint arXiv:1611.03530*.

- Zhao, J., Wang, T., Yatskar, M., Ordonez, V., and Chang, K.-W. (2017). Men also like shopping: Reducing gender bias amplification using corpus-level constraints. *arXiv preprint arXiv:1707.09457*.
- Zou, D., Cao, Y., Zhou, D., and Gu, Q. (2020). Gradient descent optimizes over-parameterized deep relu networks. *Machine Learning*, 109(3):467–492.

A Experimental Details

A.1 Two-Moon Classification: Comparison with other regularization methods

In this section, we experiment the Two-moon classification example of the main paper with different regularization techniques. The small margin between the two classes allows the network to achieve a negligible loss by only learning to discriminate along the horizontal axis. However, both axes are relevant for the data distribution, and the only reason why the second dimension is not picked up is the fact that the training data allows the learning to explain the labels with only one feature, overlooking the other. Figure 3 reveals that common regularization strategies including Weight Decay, Dropout (Srivastava et al., 2014) and Batch Normalization (Ioffe and Szegedy, 2015) do not help achieving a larger margin classifier. Unless states otherwise, all the methods are trained with Full batch Gradient Descent with a learning rate of $1e - 2$ and a momentum of 0.9 for $10k$ iterations.

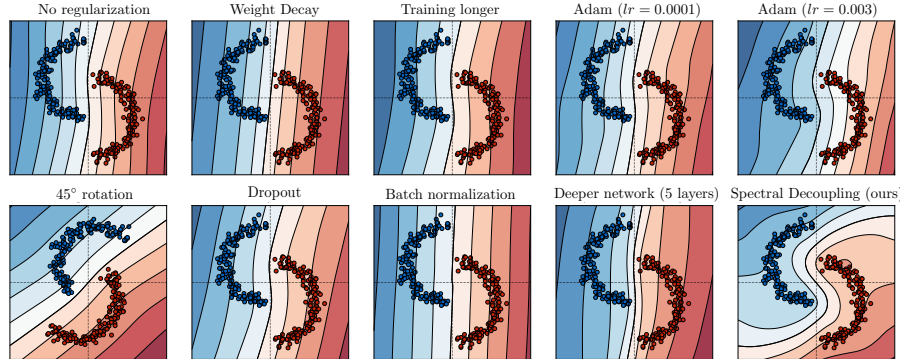


Fig. 3: The effect of common regularization methods on a simple task of two-moon classification. It can be seen that common practices of deep learning seem not to help with learning a curved decision boundary. The acronym “lr” for the Adam optimizer refers to the learning rate. Shown decision boundaries are the average over 10 runs in which datapoints and the model initialization parameters are sampled randomly. Here, only the datapoints of one particular seed are plotted for visual clarity.

A.2 Colored MNIST with color bias: Further investigation

Here we compare three methods: Empirical Risk Minimization (ERM), our proposed Spectral Decoupling (SD), and Invariant Risk Minimization (IRM) (Arjovsky et al., 2019). Recall that training data is contrived in a way that the color is highly correlated with the label. However, this correlation is reversed in the test test. For a method to achieve good performance on the test test, it should reduce its reliance on the color feature and instead focus on the digit features. As reported in Table. 1, SD and IRM performs significantly better than ERM on the test set. To investigate this, we study a trained model with each of these methods on four variants of the test environment: 1) grayscale-digit: No color channel is provided and the network should only rely on digit features. 2) colored-digit: Both color and digit are provided however the color is correlated (opposite of the training set) with the label. 3) grayscale-black: All images are grayscale and blank and hence do not provide any information. 4) colored-blank: Digit features are removed and only the color feature is kept.

As shown in Figure. 4, it is evident that ERM captures the color feature and in the absence of digit features (environment 3), network’s predictions are very confident. Recall that confidence is inversely proportional to the entropy of the predictions. At the same time, SD appears to capture the color feature too. Indeed when only the color is presented to the network, SD performs poorly as well. However, looking at the associated entropy reveals that unlike ERM, SD is not confident on its predictions. Therefore, in the case where both color and digit features are presented (environment 2), SD achieves significantly better performance. We conjecture that as a result of the decoupling between the learned features, digit features *out weight* the color feature and that results in the superior performance of SD.

Meanwhile, IRM’s strategy to achieve good test performance is different. IRM appears to not capture the color feature altogether. Specifically, when only the color is presented to a network trained with IRM, network predicts 50% accuracy with low confidence meaning that IRM is indeed “Invariant” to the color. However, bear in mind that IRM requires access to separate training environments while SD does not.

Finally, Table. 3 reports the hyper-parameters used for each method.

Method	Layers	Dim	Weight decay	LR	Anneal steps	Penalty coef
ERM	2	300	0.0	1e-4	0/2000	n/a
SD	2	300	0.0	1e-4	450/2000	2e-5
IRM	2	390	0.00110794568	0.00048985365	190/500	91257.18613115903

Table 3: Hyper-parameters used for the Colored-MNIST experiment. Hyper-parameters of IRM are obtained from their released code. “Anneal steps” indicates the number of iterations done before applying the method.

For all the experiments, we use PyTorch (Paszke et al., 2017). We also use NNGeometry George (2020) for computing NTK.

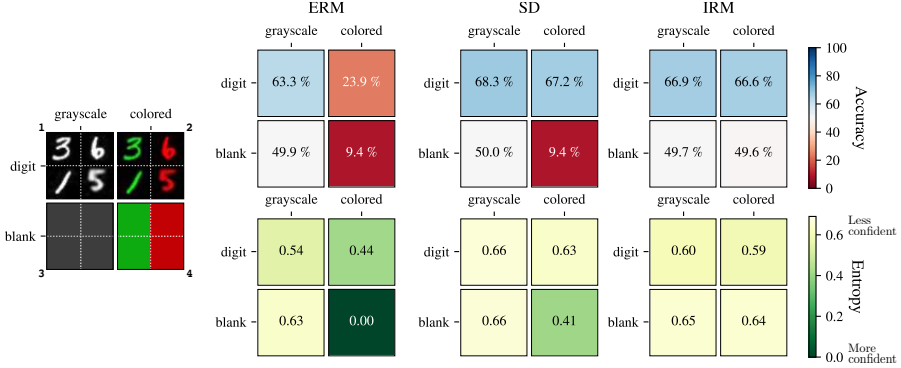


Fig. 4: Diagram comparing three learning schemes: ERM (Empirical Risk Minimization), SD (Spectral Decoupling), and IRM (Invariant Risk Minimization). **Left** shows four different environments that we test a pre-trained model on; **1) grayscale-digit**: No color channel is provided and the network should only rely on digit features. **2) colored-digit**: Both color and digit are provided however the color is correlated (opposite of the training set) with the label. **3) grayscale-blank**: All images are grayscale and blank and hence do not provide any information. **4) colored-blank**: Digit features are removed and only the color feature is kept. Each environment contains 50k testing examples. **Right** top and bottom rows show the accuracy and the entropy (inverse of confidence), respectively. **Analysis:** Compare three values of 9.4 %, 9.4 %, and 49.6 %: Both ERM and SD have learned the color feature but since it is inversely correlated with the label, when only the color feature is provided, as expected both ERM and SD performs poorly. Now compare 0.00 and 0.41: Although both ERM and SD have learned the color feature, ERM is much more confident on its predictions (zero entropy). As a consequence, when digit features are provided along with the color feature (colored-digit environment), ERM still performs poorly (23.9 %) but SD achieves significantly better results (67.2 %). Finally, note that IRM is indeed invariant to the color feature and that is because it requires access to multiple training environments.

A.3 CelebA with gender bias: The experimental details

For the CelebA experiment, we follow the same setup as in Sagawa et al. (2019) and use their released code. We use Adam optimizer for the Spectral Decoupling experiments with a learning rate of $1e - 4$ and a batch size of 128. As mentioned in the main text, for this experiment, we use a different variant of Spectral Decoupling which also provably decouples the learning dynamics,

$$\min_{\theta} \mathbf{1} \cdot \left(\log [1 + \exp (-\mathbf{Y}\hat{\mathbf{y}})] + \frac{\lambda}{2} \|\hat{\mathbf{y}} - \gamma\|^2 \right).$$

We applied a hyper-parameter search on λ and γ for each of the classes separately. Therefore, a total of four hyper-parameters are found. For class zero, $\lambda_0 = 0.088$, $\gamma_0 = 0.44$ and for class one, $\lambda_1 = 0.012$, $\gamma_1 = 2.5$ are found to result in the best worst-group performance.

B Proofs of the Theories and Lemmas

B.1 Cross-Entropy's Legendre Transformation

In this section, following [Jaakkola and Haussler \(1999\)](#), we derive the Legendre transformation of the Cross-Entropy (CE) loss function. Here, we reiterate this transformation as following,

Lemma 2 (CE's Legendre transformation, adapted from Eq. 46 of Jaakkola and Haussler (1999)). *For a variational parameter $\alpha \in [0, 1]$, the following linear lower bound holds for the cross-entropy loss function,*

$$\mathcal{L}(\omega) := \log(1 + e^{-\omega}) \geq H(\alpha) - \alpha\omega, \quad (29)$$

in which $\omega := y\hat{y}$ and $H(\alpha)$ is the Shannon's binary entropy. The equality holds for the optimal value of $\alpha^* = -\nabla_\omega \mathcal{L}$, i.e., at the maximum of r.h.s. with respect to α .

Proof. The **Legendre** transformation converts a function $\mathcal{L}(\omega)$ to another function $g(\alpha)$ of conjugate variables α , $\mathcal{L}(\omega) \rightarrow g(\alpha)$. The idea is to find the expression of the tangent line to $\mathcal{L}(\omega)$ at ω_0 which is the first-order Taylor expansion of $\mathcal{L}(\omega)$,

$$t(\omega, \omega_0) = \mathcal{L}(\omega_0) + (\omega - \omega_0)\nabla_\omega \mathcal{L}|_{\omega=\omega_0}, \quad (30)$$

where $t(\omega, \omega_0)$ is the tangent line. According to the Legendre transformation, the function $\mathcal{L}(\omega)$ can be written as a function of the intercepts of tangent lines (where $\omega = 0$). Varying ω_0 along the x -axis provides us with a general equation, representing the intercept as a function of ω ,

$$t(\omega = 0, \omega_0 = \omega) = \mathcal{L}(\omega) - \omega\nabla_\omega \mathcal{L}. \quad (31)$$

The cross-entropy loss function can be rewritten as a soft-plus function,

$$\mathcal{L}(\omega) = -\log \sigma(\omega) = \log(1 + e^{-\omega}), \quad (32)$$

in which $\omega := y\hat{y}$. Letting $\alpha := -\nabla_\omega \mathcal{L} = \sigma(-\omega)$ we have,

$$\omega = \log\left(\frac{1 - \alpha}{\alpha}\right), \quad (33)$$

which allows us to re-write the expression for the intercepts as a function of α (denoted by $g(\alpha)$),

$$g(\alpha) = \mathcal{L}(\omega) - \omega\nabla_\omega \mathcal{L} \quad (34)$$

$$= \mathcal{L}(\omega) + \alpha\omega \quad (35)$$

$$= -\alpha \log \alpha - (1 - \alpha) \log(1 - \alpha) \quad (36)$$

$$= H(\alpha), \quad (37)$$

where $H(\alpha)$ is the binary entropy function.

Now, since \mathcal{L} is convex, a tangent line is always a lower bound and therefore at its maximum it touches the original function. Consequently, the original function can be recovered as follows,

$$\mathcal{L}(\omega) = \max_{0 \leq \alpha \leq 1} H(\alpha) - \alpha\omega. \quad (38)$$

Note that the lower bound in Eq. 29 is now a linear function of $\omega := y\hat{y}$ but at the expense of an additional maximization over the variational parameter α . An illustration of the lower bound is depicted in Fig. 5. Also a comparison between the dual formulation of other common loss functions is provided in Table. 4.

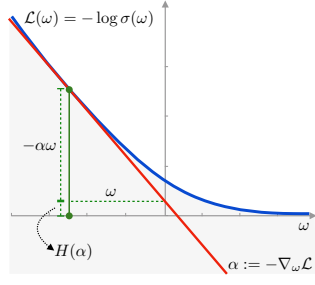


Fig. 5: Diagram illustrating the Legendre transformation of the function $\mathcal{L}(\omega) = \log(1 + e^{-\omega})$. The function is shown in blue, and the tangent line is shown in red. The tangent line is the lower bound of the function: $H(\alpha) - \alpha\omega \leq \mathcal{L}(\omega)$.

Loss	Primal form	Dual form
Cross-Entropy	$\log(1 + e^{-w})$	$\max_{0 < \alpha < 1} [H(\alpha) - \alpha\omega]$
Hinge loss	$\max(0, 1 - w)$	$\max_{0 \leq \alpha \leq 1} [\alpha\mathbf{1}^T - \alpha\omega]$
Squared error	$(1 - \omega)^2$	$\max_{\alpha} [-\frac{1}{2}\alpha^2 + \alpha - \alpha\omega]$

Table 4: Dual forms of other common different loss functions. The dual form of the Hinge loss is commonly used in Support Vector Machine (SVMs). For the ease of notation, we assume scalar ω and α .

□

B.2 Proof of Theorem 1

In this section, we present a proof of Theorem 1.

Proof. We define

$$f_i(\alpha_j) = \eta \left(\log \frac{(1 - \alpha_i)}{\alpha_i} - \frac{1}{\lambda} \sum_{jk} u_{ik} s_k^2 (u^T)_{kj} \alpha_j \right) \quad (39)$$

as the gradient function of the autonomous system equation 17.

We find the character of possible fixed points by linearization. We compute the jacobian of the gradient function evaluated at the fixed point.

$$J_{ik} = \left. \frac{df_i(\alpha_j)}{d\alpha_k} \right|_{\alpha_k^*} \quad (40)$$

$$J_{ik} = \eta \left(-\delta_{ik} [\alpha_i^*(1 - \alpha_i^*)]^{-1} - \lambda^{-1} \sum_l u_{il} s_l^2 (u^T)_{lk} \right) \quad (41)$$

The fixed point is an attractor if the jacobian is a negative-definite matrix. The first term is negative-definite matrix while the second term is negative semi-definite matrix. Since the sum of a negative matrix and negative-semi definite matrix is negative-definite, this completes the proof. \square

B.3 Proof of Lemma 1

In this section, we present a proof of Lemma 1.

Proof. Starting from the autonomous system B.3 and assumption 1, we have

$$\boldsymbol{\alpha} = \eta (-\log \boldsymbol{\alpha} - \boldsymbol{\alpha} \mathbf{A}) \quad (42)$$

where

$$\mathbf{A} = \lambda^{-1} \mathbf{U} (\mathbf{S}^2 + \lambda \mathbf{I}) \mathbf{U}^T \quad (43)$$

$$= \lambda^{-1} \begin{pmatrix} \delta^2(s_2^2 + \lambda) + (1 - \delta^2)(s_1^2 + \lambda) & \delta\sqrt{1 - \delta^2}(s_1^2 - s_2^2) \\ \delta\sqrt{1 - \delta^2}(s_1^2 - s_2^2) & \delta^2(s_1^2 + \lambda) + (1 - \delta^2)(s_2^2 + \lambda) \end{pmatrix} \quad (44)$$

Since the off-diagonal terms are of order δ , we treat them as a perturbation. The unperturbed system has a solution given by case 2

$$\boldsymbol{\alpha}^* = \begin{pmatrix} \frac{\lambda \mathcal{W}(\delta^2(\lambda^{-1}s_2^2+1)+(1-\delta^2)(\lambda^{-1}s_1^2+1))}{\delta^2(s_2^2+\lambda)+(1-\delta^2)(s_1^2+\lambda)} & \frac{\lambda \mathcal{W}(\delta^2(\lambda^{-1}s_1^2+1)+(1-\delta^2)(\lambda^{-1}s_2^2+1))}{\delta^2(s_1^2+\lambda)+(1-\delta^2)(s_2^2+\lambda)} \end{pmatrix} \quad (45)$$

We can linearize the autonomous system around the unperturbed solution to find

$$\dot{\boldsymbol{\alpha}} \simeq \eta \left(-\log(\boldsymbol{\alpha}^*) - \boldsymbol{\alpha}^* \odot \text{diag}(\mathbf{A}) + \frac{d}{d\boldsymbol{\alpha}} [-\log(\boldsymbol{\alpha}) - \boldsymbol{\alpha} \odot \text{diag}(\mathbf{A})] \Big|_{\boldsymbol{\alpha}^*} (\boldsymbol{\alpha} - \boldsymbol{\alpha}^*) \right) \quad (46)$$

$$\dot{\boldsymbol{\alpha}} \simeq \eta \left(1 - \log(\boldsymbol{\alpha}^*) - \left(\text{diag}(\mathbf{A}) + \boldsymbol{\alpha}^{*-1} \right) \odot \boldsymbol{\alpha} \right) \quad (47)$$

where we have defined $\mathbf{A} = \lambda^{-1} \mathbf{U} (\mathbf{S}^2 + \lambda \mathbf{I}) \mathbf{U}^T$.

We then apply the perturbation given by off-diagonal terms of \mathbf{A} to obtain

$$\dot{\boldsymbol{\alpha}} \simeq \eta \left(1 - \log(\boldsymbol{\alpha}^*) - \boldsymbol{\alpha} \left[\mathbf{A} + \text{diag}(\boldsymbol{\alpha}^{*-1}) \right] \right) \quad (48)$$

Solving for $\dot{\boldsymbol{\alpha}} = 0$, we obtain the solution

$$\tilde{\boldsymbol{\alpha}}^* = (1 - \log(\boldsymbol{\alpha}^*)) \left[\mathbf{A} + \text{diag}(\boldsymbol{\alpha}^{*-1}) \right]^{-1}. \quad (49)$$

\square

B.4 Proof of Theorem 2

In this section, we present a proof of Theorem 2.

Proof. From lemma 1, and with \mathbf{U} given by equation 23, we can invert \mathbf{U} and find that the perturbatory solution for the fixed point is

$$\begin{aligned}\hat{\alpha}_1^* &= \left[\lambda \left(W \left(\frac{\lambda + \delta^2 (s_1^2 - s_2^2) + s_2^2}{\lambda} \right) + 1 \right) \left(\delta \sqrt{1 - \delta^2} (s_2^2 - s_1^2) + \lambda e^{W \left(\frac{\lambda + \delta^2 (s_1^2 - s_2^2) + s_2^2}{\lambda} \right)} \right. \right. \\ &\quad \left. \left. \left(W \left(\frac{\lambda + \delta^2 (-s_1^2) + \delta^2 s_2^2 + s_1^2}{\lambda} \right) + 1 \right) \right) \right] \delta^2 (\delta^2 - 1) (s_1^2 - s_2^2)^2 + \\ &\quad \left(\lambda + \delta^2 (s_1^2 - s_2^2) + \lambda e^{W \left(\frac{\lambda + \delta^2 (s_1^2 - s_2^2) + s_2^2}{\lambda} \right)} + s_2^2 \right) \\ &\quad \left. \left(\lambda + \delta^2 s_2^2 - (\delta^2 - 1) s_1^2 + \lambda e^{W \left(\frac{\lambda + \delta^2 (-s_1^2) + \delta^2 s_2^2 + s_1^2}{\lambda} \right)} \right) \right]^{-1} \\ \hat{\alpha}_2^* &= \left[\lambda \left(W \left(\frac{\lambda + \delta^2 (-s_1^2) + \delta^2 s_2^2 + s_1^2}{\lambda} \right) + 1 \right) \left(\delta \sqrt{1 - \delta^2} (s_2^2 - s_1^2) + \lambda e^{W \left(\frac{\lambda + \delta^2 (-s_1^2) + \delta^2 s_2^2 + s_1^2}{\lambda} \right)} \right. \right. \\ &\quad \left. \left. \left(W \left(\frac{\lambda + \delta^2 (s_1^2 - s_2^2) + s_2^2}{\lambda} \right) + 1 \right) \right) \right] \\ &\quad \left[\delta^2 (\delta^2 - 1) (s_1^2 - s_2^2)^2 + \left(\lambda + \delta^2 (s_1^2 - s_2^2) + \lambda e^{W \left(\frac{\lambda + \delta^2 (s_1^2 - s_2^2) + s_2^2}{\lambda} \right)} + s_2^2 \right) \right. \\ &\quad \left. \left(\lambda + \delta^2 s_2^2 - (\delta^2 - 1) s_1^2 + \lambda e^{W \left(\frac{\lambda + \delta^2 (-s_1^2) + \delta^2 s_2^2 + s_1^2}{\lambda} \right)} \right) \right]^{-1}\end{aligned}$$

We have found at equation 18 that the corresponding steady-state feature response is given by

$$\hat{\mathbf{z}}^* = \frac{1}{\lambda} \mathbf{S}^2 \mathbf{U}^T \tilde{\boldsymbol{\alpha}}^* \quad (50)$$

In the perturbatory regime δ is taken to be a small parameter. We therefore perform a first-order Taylor series expansion of $\hat{\mathbf{z}}^*$ around $\delta = 0$ to obtain

$$\begin{aligned}\hat{z}_1^* &= \frac{\delta s_1^2 \left(W \left(\frac{\lambda + s_2^2}{\lambda} \right) + 1 \right) \left(\lambda + \lambda e^{W \left(\frac{\lambda + s_2^2}{\lambda} \right)} + s_2^2 \right)}{\left(\lambda + \lambda e^{W \left(\frac{\lambda + s_1^2}{\lambda} \right)} + s_1^2 \right) \left(\lambda + \lambda e^{W \left(\frac{\lambda + s_2^2}{\lambda} \right)} + s_2^2 \right)} + \frac{\lambda s_1^2 e^{W \left(\frac{\lambda + s_2^2}{\lambda} \right)} \left(W \left(\frac{\lambda + s_1^2}{\lambda} \right) + 1 \right) \left(W \left(\frac{\lambda + s_2^2}{\lambda} \right) + 1 \right)}{\left(\lambda + \lambda e^{W \left(\frac{\lambda + s_1^2}{\lambda} \right)} + s_1^2 \right) \left(\lambda + \lambda e^{W \left(\frac{\lambda + s_2^2}{\lambda} \right)} + s_2^2 \right)} \\ &\quad (51)\end{aligned}$$

$$\begin{aligned}\hat{z}_2^* &= \frac{\lambda s_2^2 e^{W \left(\frac{\lambda + s_1^2}{\lambda} \right)} \left(W \left(\frac{\lambda + s_1^2}{\lambda} \right) + 1 \right) \left(W \left(\frac{\lambda + s_2^2}{\lambda} \right) + 1 \right)}{\left(\lambda + \lambda e^{W \left(\frac{\lambda + s_1^2}{\lambda} \right)} + s_1^2 \right) \left(\lambda + \lambda e^{W \left(\frac{\lambda + s_2^2}{\lambda} \right)} + s_2^2 \right)} - \frac{\delta s_2^2 \left(W \left(\frac{\lambda + s_1^2}{\lambda} \right) + 1 \right) \left(\lambda + \lambda e^{W \left(\frac{\lambda + s_2^2}{\lambda} \right)} + s_1^2 \right)}{\left(\lambda + \lambda e^{W \left(\frac{\lambda + s_1^2}{\lambda} \right)} + s_1^2 \right) \left(\lambda + \lambda e^{W \left(\frac{\lambda + s_2^2}{\lambda} \right)} + s_2^2 \right)} \\ &\quad (52)\end{aligned}$$

Taking the derivative of \hat{z}_2^* with respect to \tilde{s}_1 , we find

$$\frac{d\hat{z}_2^*}{ds_1^2} = -\frac{\delta\lambda s_2^2 \left(e^{W\left(\frac{\lambda+s_1^2}{\lambda}\right)} - e^{W\left(\frac{\lambda+s_2^2}{\lambda}\right)} \right) \left(W\left(\frac{\lambda+s_1^2}{\lambda}\right) + 1 \right)}{\left(\lambda + \lambda e^{W\left(\frac{\lambda+s_1^2}{\lambda}\right)} + s_1^2 \right)^2 \left(\lambda + \lambda e^{W\left(\frac{\lambda+s_2^2}{\lambda}\right)} + s_2^2 \right)} \quad (53)$$

Knowing that the exponential of the W Lambert function is a strictly increasing function and that $s_1^2 > s_2^2$, we find

$$\frac{d\hat{z}_2^*}{ds_1^2} < 0. \quad (54)$$

□

C Additional Experiments

In this section, we provide a few more experiments to study the difference between the primal and dual form dynamics. We also compare the learning dynamics in cases with and without Spectral Decoupling (SD).

Recall that primal dynamics arise from the following optimization,

$$\min_{\theta} \mathbf{1} \cdot \left(\log [1 + \exp(-\mathbf{Y}\hat{\mathbf{y}})] + \frac{\lambda}{2} \|\hat{\theta}\|^2 \right),$$

while the dual dynamics as the result of another optimization,

$$\max_{\alpha_i} \left[H(\alpha) - \frac{1}{2\lambda} \sum_{jq} \alpha \mathbf{Y} \Phi_0 \Phi_0^T \mathbf{Y}^T \alpha^T \right].$$

Also recall that Spectral Decoupling suggests the following optimization,

$$\min_{\theta} \mathbf{1} \cdot \left(\log [1 + \exp(-\mathbf{Y}\hat{\mathbf{y}})] + \frac{\lambda}{2} \|\hat{\mathbf{y}}\|^2 \right).$$

Here, we conduct experiments on a simple toy classification with two data points for which the matrix \mathbf{U} of Eq. 23 is defined as, $\mathbf{U} = \begin{pmatrix} 0.8 & -0.6 \\ 0.6 & 0.8 \end{pmatrix}$. The corresponding singular values $\mathbf{S} = [s_1, s_2 = 2]$ where $s_1 \in \{2, 3, 4, 5, 6\}$. According to Eq. 21, when $\mathbf{S} = [2, 2]$, the dynamics decouple while in other cases starvation occurs. Figure. 6 shows the corresponding features of z_1 and z_2 . It is evident that by increasing the value of s_1 , the value of z_1^* increases while z_2^* decreases (starves). Figure. 6 (left) also compares the difference between the primal and the dual dynamics. Note that although their dynamics are different, they both share the same fixed points. Figure. 6 (right) also shows that Spectral Decoupling (SD) indeed decouples the learning dynamics of z_1 and z_2 and hence increasing the corresponding singular value of one does not affect the other.

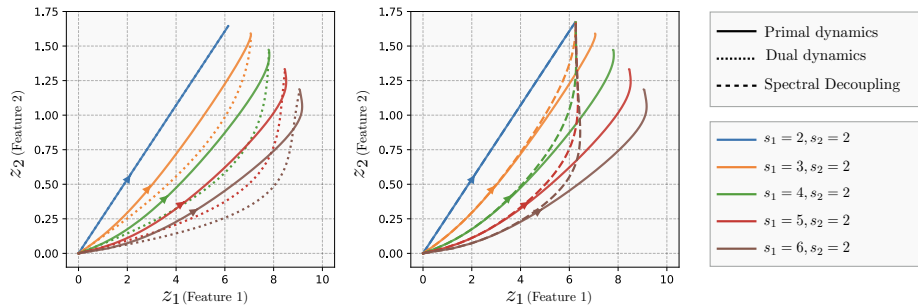


Fig. 6: An illustration of the learning dynamics for a simple 2D classification task. x-axis and y-axis represent learning along features of z_1 and z_2 , respectively. Each trajectory corresponds to a combination of the corresponding singular values of s_1 and s_2 . It is evident that by increasing the value of s_1 , the value of z_1^* increases while z_2^* decreases (starves). (**Left**) compares the difference between the primal and the dual dynamics. Note that although their dynamics are different, they both share the same fixed points. (**Right**) shows that Spectral Decoupling (SD) indeed decouples the learning dynamics of z_1 and z_2 and hence increasing the corresponding singular value of one does not affect the other.